Fuel 310 (2022) 122459

Contents lists available at ScienceDirect

Fuel

journal homepage: www.elsevier.com/locate/fuel

Full Length Article

Cooperative Brønsted-Lewis acid sites created by phosphotungstic acid encapsulated metal–organic frameworks for selective glucose conversion to 5-hydroxymethylfurfural

Mohammad Shahinur Rahaman [a], Sarttrawut Tulaphol [a,b], Md Anwar Hossain [a], Jacek B. Jasinski [c], Ning Sun [d,e], Anthe George [f,g], Blake A. Simmons [d,g], Thana Maihom [h], Mark Crocker [i,j], Noppadon Sathitsuksanoh [a,*]

[a] Department of Chemical Engineering, University of Louisville, Louisville, KY 40292, USA
[b] Sustainable Polymer & Innovative Composite Materials Research Group, Department of Chemistry, Faculty of Science, King Mongkut's University of Technology Thonburi, Bangkok 10140, Thailand
[c] Conn Center for Renewable Energy Research, University of Louisville, Louisville, KY 40292, USA
[d] Lawrence Berkeley National Laboratory, Berkeley, CA 94720, USA
[e] Advanced Biofuels and Bioproducts Process Demonstration Unit, Emeryville, CA 94608, USA
[f] Sandia National Laboratories, 7011 East Ave, Livermore, CA 94551, USA
[g] Joint BioEnergy Institute, Emeryville, CA 94608, USA
[h] Department of Chemistry, Faculty of Liberal Arts and Science, Kasetsart University, Kamphaeng Saen Campus, Nakhon Pathom 73140, Thailand
[i] Center for Applied Energy Research, University of Kentucky, 2540 Research Park Drive, Lexington, KY 40511, USA
[j] Department of Chemistry, University of Kentucky, Lexington, KY 40506, USA

ARTICLE INFO

Keywords:
Metal-organic frameworks
Phosphotungstic acid
Encapsulation
Glucose dehydration
Hydroxymethylfurfural
Cooperative

ABSTRACT

Production of 5-hydroxymethylfurfural (HMF) from biomass-derived glucose has great potential for synthesis of renewable fuels and chemicals. Selective glucose conversion to 5-hydroxymethylfurfural requires a balance between Lewis and Brønsted acids for the cascade of glucose isomerization followed by fructose dehydration. A dual Brønsted-Lewis acid, phosphotungstic acid encapsulated MIL-101(Al)–NH_2 metal–organic frameworks (MOFs) was developed to catalyze the glucose dehydration reaction. The encapsulated catalysts had a high HMF selectivity of 58% at 44% glucose conversion at 120 °C in $[C_4C_1im]Cl$. Phosphotungstic acid was uniformly dispersed in the MOF pores, which provided both Brønsted and Lewis acid sites for this cascade reaction. The Brønsted acidic phosphotungstic acid-encapsulated MOF catalyst was stable and recyclable at least four times. These findings explain the effect of phosphotungstic acid location for maximizing the HMF selectivity and suggest a new approach for the design of bifunctional solid acid catalysts for selective HMF production from glucose. Moreover, the tunability of the acid properties of the encapsulated MOF catalysts provides opportunities for other biomass transformations.

1. Introduction

Negative consequences of fuel and chemical production from petroleum, especially sizeable greenhouse gas emissions, price volatility [1], and non-renewability [2], have propelled the production of commodity chemicals from renewable plant biomass. Hydroxymethylfurfural (HMF) is a versatile platform chemical derived from biomass with potential applications for fuels, chemicals, plastics, and pharmaceuticals [3-5]. The challenge of glucose dehydration to HMF is to obtain high HMF selectivity. Although the glucose dehydration reaction has been studied extensively, its mechanism is still being debated [6,7].

In general, glucose dehydration to HMF can occur by two chemical pathways (Scheme 1), direct dehydration (path 1) and tandem isomerization-dehydration reactions (path 2). The direct dehydration of glucose to HMF by Brønsted acid catalysts is slow, and HMF selectivity is low because of side reactions such as cross-condensation with formation of undesired humins [8-11]. Tandem isomerization-dehydration

* Corresponding author.
E-mail address: N.sathitsuksanoh@louisville.edu (N. Sathitsuksanoh).

https://doi.org/10.1016/j.fuel.2021.122459
Received 18 June 2021; Received in revised form 3 October 2021; Accepted 28 October 2021
Available online 12 November 2021

reactions in one-pot afford opportunities to transform glucose to HMF selectively [12]. Selective production of HMF from glucose requires cooperation between Lewis and Brønsted acid catalysts for glucose isomerization to fructose and subsequent fructose dehydration to HMF [8,13-15]. Lewis acid promotes the isomerization of glucose to fructose and then dehydration of fructose to HMF by Brønsted acid [16-18].

Swift et al. demonstrated this concept of tandem isomerization-dehydration reactions by incorporating a Lewis acid ($CrCl_3$) with a Brønsted acid (HCl) catalyst, an approach that enhanced both catalytic activity for glucose dehydration and HMF selectivity [19]. Vieira et al. used the combination of Lewis acid Nb_2O_5 and Bronsted acid HCl in a water/tetrahydrofuran (THF) biphasic system. They found that the Brønsted acid HCl was necessary to improve HMF selectivity from 7.6% to 51% and glucose conversion from 49% to 93%, compared with Nb_2O_5 alone [18]. Nikolla et al. used the combination of Sn-containing β-zeolite and HCl in H_2O/THF biphasic system to reach 72% HMF selectivity at 79% glucose conversion [20]. However, all these studies were conducted with homogeneous Brønsted acid catalysts that complicate product purification [21] and catalyst recycling. Therefore, it would be most useful to have solid catalysts that possess both Brønsted and Lewis acid active sites for selective glucose conversion to HMF. In answer to this need, this report describes metal–organic frameworks that have both Brønsted and Lewis acid sites for selective glucose conversion to HMF.

Metal-organic frameworks (MOFs) are porous crystalline materials that consist of metal ions or clusters coordinated with organic linkers to form highly uniform solid networks [22-27]. The coordinated unsaturated metal sites (cus) endow MOFs with Lewis acidity [28,29]. Lewis acid sites of MOFs have been used to catalyze various reactions, such as aldol condensation [30], deacetalization-Knoevenagel condensation [31,32], Meinwald rearrangement [33], and CO oxidation [34]. The porosity of MOFs enables incorporation of large Brønsted acidic molecules to create bifunctional acid catalysts for various acid-catalyzed organic reactions [22,23,35-38].

Polyoxometalates (POMs) are versatile catalysts because of their many active sites [39,40]. The Keggin family of POMs ($[XM_{12}O_{40}]^{n-}$ anions (X = Si and P, M = Mo and W) with protons as the only countercations are heteropolyacids; examples include phosphotungstic acid, silicotungstic acid, silicomolybdic acid, and phosphomolybdic acid. These heteropolyacids have high acid strength and they are less corrosive compared with ordinary mineral acids (HBr, H_2SO_4, HNO_3, and HCl) [41,42]. Although these properties make heteropolyacids attractive in acid-catalyzed reactions [43-47], they are soluble in water and many organic solvents. Thus, they are difficult to recycle, and their presence complicates purification of soluble products.

Trapping heteropolyacids in MOF pores generates bifunctional catalysts with both Lewis and Brønsted acids, which are important for selective glucose conversion to HMF [15,48]. Indeed, as reported in Table S1, the Keggin-type heteropolyacids have been encapsulated successfully in the pores of MOFs [49-52]. For example, phosphotungstic acid (PTA)-encapsulated MIL-101(Cr) was used for various catalytic reactions such as the esterification of *n*-butanol with acetic acid [53], dehydration of methanol [53], oxidative desulfurization of dibenzothiophene[54], carbohydrate dehydration to 5-hydroxymethylfurfural [52], and oxidation of the alkenes [55]. Zhang et al. synthesized PTA⊂MIL-101(Cr) by encapsulating PTA in MIL-101(Cr) for sugar dehydration [52]. Fructose dehydration by PTA⊂MIL-101(Cr) was selective for HMF (77% HMF selectivity at 82% fructose conversion). However, PTA⊂MIL-101(Cr) was not selective for HMF in glucose dehydration (10% HMF selectivity at 21% glucose conversion). Moreover, the use of fructose as a feedstock is not cost-effective because glucose is less expensive than fructose [56]. In addition, the chromium in PTA⊂MIL-101(Cr) catalysts is harmful to humans, animals, and the environment [57]. Therefore, there is a need to develop heterogeneous chromium-free acid catalytic systems that possess both Brønsted and Lewis acid sites to regulate the HMF selectivity in glucose dehydration.

Here, this work describes encapsulation of phosphotungstic acid in the pores of MIL-101(Al)–NH_2 to form PTA⊂MIL-101(Al)–NH_2. The effect of PTA encapsulation on catalytic performance in glucose dehydration with $[C_4C_1im]Cl$ as solvent was evaluated. The $[C_4C_1im]Cl$ was selected as the reaction solvent because our previous studies established that the alkyl imidazolium chloride ionic liquids, such as $[C_2C_1im]Cl$ and $[C_4C_1im]Cl$, can dissolve cellulose and enable hydrolysis of cellulose to sugars [58-60]. The MIL-101(Al)–NH_2 was selected because it is chemically and thermally stable [32]. Moreover, Brønsted acidic PTA was used as the heteropolyacid because it has a high acid strength compared with other heteropolyacids [61]. The encapsulated PTA in MIL-101(Al)–NH_2 was uniformly dispersed and stable in MIL-101(Al)-NH_2 pores, and it provided Brønsted acid sites that rendered the catalyst selective for HMF production. These results reveal the unrecognized catalytic performance of the PTA⊂MIL-101(Al)–NH_2 catalysts for selective glucose dehydration.

2. Materials and methods

2.1. Materials

The following chemicals were purchased and used as received: D-glucose, 1-butyl-3-methylimidazolium chloride ($[C_4C_1im]Cl$), 2-aminoterephthalic acid (2-ATA), aluminum chloride hexahydrate, phosphotungstic acid (PTA), and *N,N*-dimethylformamide (DMF), methanol, ethanol, n-propanol, 2-propanol, n-butanol, 2-butanol, *p*-dioxane, ethyl acetate (EA), *N,N*-dimethylformamide (DMF), *N,N*-dimethylacetamide (DMA), dimethyl sulfoxide (DMSO), and tetrahydrofuran (THF). Table S2 summarizes the list of chemicals/reagents, their supplier, purity, and CAS number. All other chemicals, solvents, and gases were of

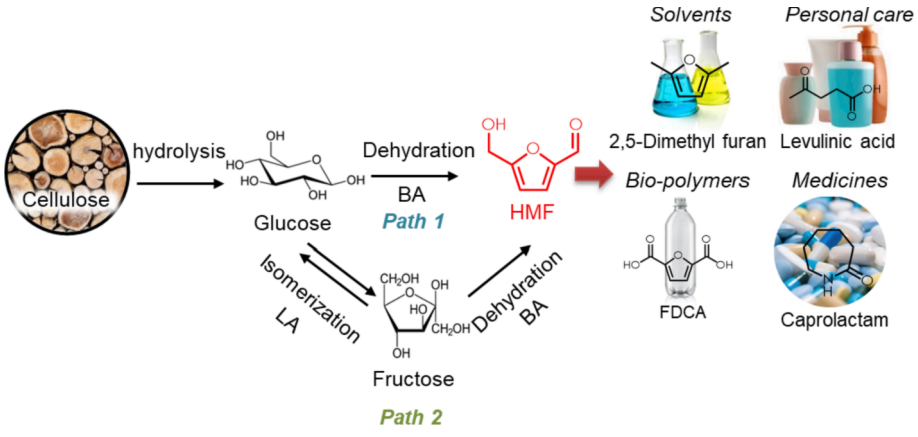

Scheme 1. Reaction network of HMF production (BA = Brønsted acid, LA = Lewis acid).

the highest purity available from commercial sources.

2.2. Synthesis of metal–organic frameworks

2.2.1. Synthesis of MIL-101(Al)–NH_2

MIL-101(Al)–NH_2 was synthesized by the solvothermal method with a slight modification [30]. Typically, a mixture of aluminum chloride hexahydrate (0.51 g, 2.1 mmol) and 2-aminoterephthalic acid (0.56 g, 3.1 mmol) in DMF (30 mL) was kept in a Teflon-lined autoclave reactor without stirring at 130 °C for 72 h. Then the reactor was cooled to ambient temperature, and the solids were separated from the solution by centrifugation (6000 RPM, 5 min). The solids were washed with DMF under sonication for 10 min. Finally, the solid catalysts were washed three times with methanol at room temperature followed by washing with hot (70 °C) methanol for 5 h and dried overnight under vacuum at 80 °C.

2.2.2. Synthesis of encapsulated PTA in MIL-101(Al)–NH_2 (PTA⊂MIL-101(Al)–NH_2)

PTA⊂MIL-101(Al)–NH_2 was synthesized by incorporating phosphotungstic acid (PTA) hydrated during the synthesis of MIL-101(Al)–NH_2. In short, aluminum chloride hexahydrate (0.51 g, 2.1 mmol), 2-amino terephthalic acid (0.56 g, 3.1 mmol), and different amounts of PTA hydrate (0.1–2.0 g) in DMF (30 mL, ρ = ~0.9 g/mL) were kept in a Teflon-lined autoclave reactor without stirring, and the mixture was heated at 130 °C for 72 h. After cooling to ambient temperature, the resulting solids were separated by centrifugation (6000 RPM, 5 min), washed with DMF, then washed with hot methanol (70 °C), and finally washed with acetone, and dried under vacuum at 80 °C overnight.

2.3. Catalyst characterization

2.3.1. Transmission electron microscopy and energy-dispersive X-ray spectroscopy analysis

The microstructure and elemental distribution of the metal–organic frameworks (MOFs) were analyzed using transmission electron microscopy (TEM) in a Tecnai F20 (FEI company, OR, USA) microscope operating at 200 kV. TEM specimens were prepared by dispersing small amounts of catalysts onto Cu grid-supported holey carbon films. For the analysis of the microstructure, scanning transmission electron microscopy (STEM) images were acquired with a high annular angle dark field (HAADF) detector (E.A. Fischione Instruments, Inc., PA, USA) and an electron probe of a 1 nm diameter. For the elemental distribution analysis, energy-dispersive X-ray spectroscopy (EDS) maps were collected using a TEAM EDS (EDAX, Inc., NJ, USA) spectrometer.

2.3.2. N_2 adsorption–desorption

The N_2 adsorption–desorption assay was conducted with a Micromeritics Tristar (Norcross, GA, USA) instrument. The function of TriStar was verified with reference materials (Micromeritics). Prior to the measurement, the samples were pretreated with a Micromeritics FlowPrep with sample degasser (Norcross, GA, USA) at 160 °C for 2 h. The surface area, S_{BET}, was determined from N_2 isotherms using the Brunauer–Emmett–Teller equation (BET) at −196.15 °C (77 K) [62,63]. The BET model assumes multilayer gas adsorption on the adsorbent's surface and obtains the sample surface area value by determining the monolayer volume of adsorbed gas from the isotherm data [64,65]. BET surface area was calculated at relative pressures between 0.05 and 0.3. The pore volume and size were calculated from the N_2 desorption values based on the Barrett–Joyner–Halenda (BJH) model [66-68]. The BJH model determines the mesopore volume distribution, which accounts for the change in adsorbate layer thickness and the liquid condensed in the pores [69]. The pore volume was calculated as the uptake (cm^3/g) at a relative pressure of 0.95.

2.3.3. Thermogravimetric analysis

Thermogravimetric analysis (TGA) was performed on an SDT Q600 TA instrument (New Castle, DE, USA). The TGA profiles were used to characterize the thermal stability of MOFs. About 20 mg of sample was placed in a cylindrical alumina crucible and heated in static air from ambient temperature to 700 °C with a nominal heating rate of 10 °C/min. The change in weight of MOF samples was used to determine the moisture content, decomposition of the linkers, and formation of metal oxides.

2.3.4. Fourier transform infrared spectroscopy

Infrared spectra of the synthesized catalysts were recorded on a JASCO Fourier transform infrared (FTIR) spectrometer (Easton, MD, USA), equipped with an attenuated total reflection stage (ATR). Samples of about 5 mg were used in each analysis. The sample was scanned in the spectral range between 400 and 4000 cm^{-1} at a 4 cm^{-1} resolution. Spectra were collected using a deuterated triglycine sulfate (DTGS) detector averaging 256 scans.

2.3.5. Diffuse reflectance infrared Fourier transform spectroscopy

Diffuse reflectance infrared Fourier transform spectroscopy (DRIFTS) with adsorbed pyridine was performed to characterize acid sites; measurements were made with a JASCO FTIR-4700 equipped with high temperature DiffuseIR™ cell (PIKE Technology, WI, USA). The protocol for the DRIFTS experiments with temperature programmed desorption is described elsewhere and used with a slight modification [70,71]. In short, MOF samples (~5 mg) were placed in a cylindrical alumina crucible and treated in nitrogen gas (50 mL/min) at 150 °C for 30 min unless otherwise noted. After the treatment, the DRIFT spectra of MOF catalysts were recorded as the background spectra. The MOF catalysts were then saturated with pyridine vapor in the low of N_2 gas (50 mL/min). The adsorbed pyridine was removed by flushing with N_2 gas (50 mL/min) at 50, 100, or 150 °C for 30 min before recording the DRIFT spectra. All spectra were recorded with 256 scans between 4000 and 400 cm^{-1} at a 4 cm^{-1} resolution using a mercury cadmium telluride (MCT) detector cooled with liquid nitrogen. The ratio of Brønsted acid to Lewis acid sites (B/L) was calculated from the integrated area of the bands (after background subtraction) of adsorbed pyridine at 1067 and 1030 cm^{-1} [72].

2.3.6. X-ray diffraction

X-ray diffraction of MOFs was conducted with a Bruker AXS Model D8 Advance A28 diffractometer (Germany) using CuK_α radiation in the 2θ range from 5° to 40° with 0.02°/step. Samples of about 200 mg were used in each analysis.

2.3.7. Inductively coupled plasma-optical emission spectroscopy

Inductively coupled plasma-optical emission spectroscopy (ICP-OES) measurements were performed using a 100 mg sample dissolved in 10 mL of nitric acid. Heating was used to ensure that the sample was completely dissolved. Once cooled, the sample was further diluted to 25 mL with double distilled water. Measurements were acquired on a Varian 720-ES spectrometer equipped with a seaspray nebulizer and cyclonic class spray chamber. Parameters included a sample intake of 1 mL/min, argon plasma flow rate of 15 L/min, and an auxiliary gas (Ar) flow rate of 1.5 L/min. The instrument was calibrated using a certified reference materials (CRMs) manufactured by VHG.

2.4. Dehydration of glucose

A 50 mg sample of glucose and 1 g [C_4C_1im]Cl were added to a 25 mL pressure tube. The catalyst was loaded with respect to the glucose at a glucose:Al molar ratio of 25:1 unless otherwise noted. The pressure tube was sealed, stirred at 700 RPM (to minimize mass transfer limitations) and kept in an oil bath at 120 °C unless otherwise noted. The reaction was stopped by quenching in a cold-water bath, followed by adding

water (~5 mL) to dissolve the remaining glucose and prevent the solidification of ionic liquid. The solution was centrifuged and the residual solids were removed. The liquid sample was withdrawn and analyzed for changes in glucose and the occurrence of dehydration products.

2.5. Product analysis and quantification

The reactants and products were analyzed by a High-Performance Liquid Chromatography (HPLC, Agilent Technology, Santa Clara, CA, USA) equipped with a refractive index detector (RID) and diode array detector (DAD). An Aminex HPX-87H column (300 × 7.8 mm, Bio-Rad®, Hercules, CA, USA) was used for reactant and product separation at 60 °C with 0.6 mL/min of 4 mM H_2SO_4 as the mobile phase. The concentrations of sugars and other products were determined by the peak areas from the RID signals. The main HMF product was determined by the peak area from the DAD signals at 280 nm. Sugar and reaction products were calibrated against certified standards (Absolute Standards, Inc., Hamden, CT, USA). The glucose conversion, product yield, and product selectivity were calculated as follows:

$$\text{Glucose conversion}\ (\%) = \frac{\text{mole of glucose reacted}}{\text{initial mole of glucose}} \times 100$$

$$\text{Product yield}\ \ (\%) = \frac{\text{mole of product generated}}{\text{initial mole of glucose}} \times 100$$

$$\text{Product selectivity}\ \ (\%) = \frac{\text{Product yield}}{\text{Glucose conversion}} \times 100$$

To ensure that the determination of glucose conversion and HMF selectivity were accurate, control experiments using PTA⊂MIL-101(Al)–NH_2, ionic liquid, and water were conducted at ambient temperature for 2 h. The change in glucose and HMF concentrations in the presence of MOFs was negligible (*see Supplementary Materials and Fig. S1 for detail*). Moreover, to confirm the formation of HMF, solvent extraction by ethyl acetate was used with the reaction solution. The extracted solution was analyzed by Agilent gas chromatography-mass spectrometry (GC–MS, model 7890A and 5977A, Agilent Technologies, Santa Clara, CA, USA) equipped with a DB-1701 column (Agilent Technologies, 30 m × 0.25 mm id, 0.25 μm) (*see Supplementary Materials and Fig. S2 for detail*).

3. Results

Encapsulating phosphotungstic acid (PTA) in MIL-101(Al)–NH_2 (Al-MOF) formed encapsulated PTA⊂MIL-101(Al)–NH_2 (PTA⊂Al-MOF) catalysts. The effect of PTA loading on MOF physicochemical and acid properties was investigated. Subsequently, the efficiency of PTA⊂Al-MOF catalysis of glucose dehydration was measured by comparing the performance of encapsulated PTA catalysts with different PTA loading.

3.1. Physicochemical properties of the PTA⊂MIL-101(Al)–NH_2 catalyst

To evaluate the physicochemical properties of the encapsulated PTA⊂Al-MOF catalysts, first, an N_2 adsorption–desorption was performed to measure the surface area and pore volume (Fig. S3A). The bare Al-MOF exhibited a Type IV isotherm, which suggested that the MIL-101(Al)–NH_2 catalyst was mesoporous. On the basis of the isotherms, the MOF total surface area and pore volume were calculated and shown in Table 1. As a control, the surface area and pore volume of Al-MOF were 1487 m^2/g and 0.92 cc/g, similar to reported values [73,74]. As expected, an increase in PTA loading decreased both total surface area and pore volume, which indicated that the encapsulated PTA occupied the pores of the Al-MOF. The average pore diameter of the synthesized catalysts was ~ 2.4–2.7 nm, in agreement with reported values of 1.6–2.9 nm [32,75]. The critical diameter for D-glucose was ~ 0.84–0.85 nm [76], which is sufficiently small to enable access to the active sites within the MOF structure.

Next, X-ray diffraction (XRD) was conducted to determine the crystallinity of the encapsulated PTA⊂Al-MOF catalysts (Fig. S3B). As a control, the X-ray diffractogram of the PTA exhibited unique peaks at 7.2° and 9.0°, similar to reported values [77]. The consistency between the diffractograms of the encapsulated PTA⊂Al-MOF catalysts and bare Al-MOF suggested that, during synthesis, the PTA⊂Al-MOF catalysts retained the structural integrity of the MIL-101 framework. These PTA peaks were not observed in the encapsulated PTA⊂Al-MOF catalysts, which suggested that PTA was well dispersed in the pores of Al-MOF [77] and/or the PTA clusters in the pentagonal and hexagonal windows of Al-MOF were indeed smaller than 1.2–1.6 nm [77-79]. Interestingly, the PTA⊂Al-MOF catalysts showed slightly broader XRD peaks and a shoulder (~11°). The peak broadening and occurrence of the shoulder was hypothesized to be due to the interaction of the encapsulated PTA clusters with the MIL-101 framework, which resulted in changes in the symmetry of the clusters in the MOF cages. Previous studies using POM-encapsulated MIL-101 MOFs showed similar XRD peak broadening [29,30,52,55,80,81]. To measure PTA dispersion in the Al-MOF catalyst's pore structure, the encapsulated 14%PTA⊂Al-MOF catalyst was imaged by STEM-HAADF. As a control, the STEM-HAADF image and elemental mapping of the bare Al-MOF showed that it was highly porous with dispersed Al (Fig. 1A and B). The STEM-HAADF image and elemental composition mapping of aluminum (Al) and tungsten (W) of the 14%PTA⊂Al-MOF showed a highly porous and uniform distribution of W and Al clusters within the Al-MOF catalyst (Fig. 1C-F), which confirmed our XRD data which indicated that PTA was highly dispersed in the pores of the Al-MOF catalyst.

To determine the surface functionality of the synthesized catalysts,

Table 1
Physicochemical properties of MOFs with varying PTA content.

Entry	PTA loading [g/30 mL][a]	Catalyst[b]	Al [wt. %][c]	W [wt. %][c]	PTA [wt. %][c]	Al/W [mol/mol]	B/L[d]	S_{BET} [m^2/g]	Total pore volume [cm^3/g]	Pore diameter (nm)
1	0.00	MIL-101(Al)-NH_2	11.56	–		–	0.37	1487	0.92	2.49
2	0.10	8%PTA⊂MIL-101 (Al)-NH_2	9.33	6.2	8.1	10.3	0.53	1375	0.82	2.39
3	0.25	14%PTA⊂MIL-101 (Al)-NH_2	9.53	11.03	14.3	5.9	0.78	1276	0.78	2.46
4	0.50	15%PTA⊂MIL-101 (Al)-NH_2	9.19	11.51	15.0	5.4	0.96	1061	0.72	2.72
5	1.00	17%PTA⊂MIL-101 (Al)-NH_2	9.64	13.00	16.9	5.1	1.04	961	0.59	2.45
6	2.00	18%PTA⊂MIL-101 (Al)-NH_2	9.11	13.52	17.5	4.6	1.14	854	0.57	2.69

[a] Per 30 mL DMF.
[b] Number before catalyst name indicates the wt.% of encapsulated PTA measured by ICP-OES.
[c] Composition measured by ICP-OES.
[d] B/L indicates Brønsted acid/Lewis acid site ratio from the area integral by diffuse reflectance infrared Fourier transform spectroscopy (DRIFTS).

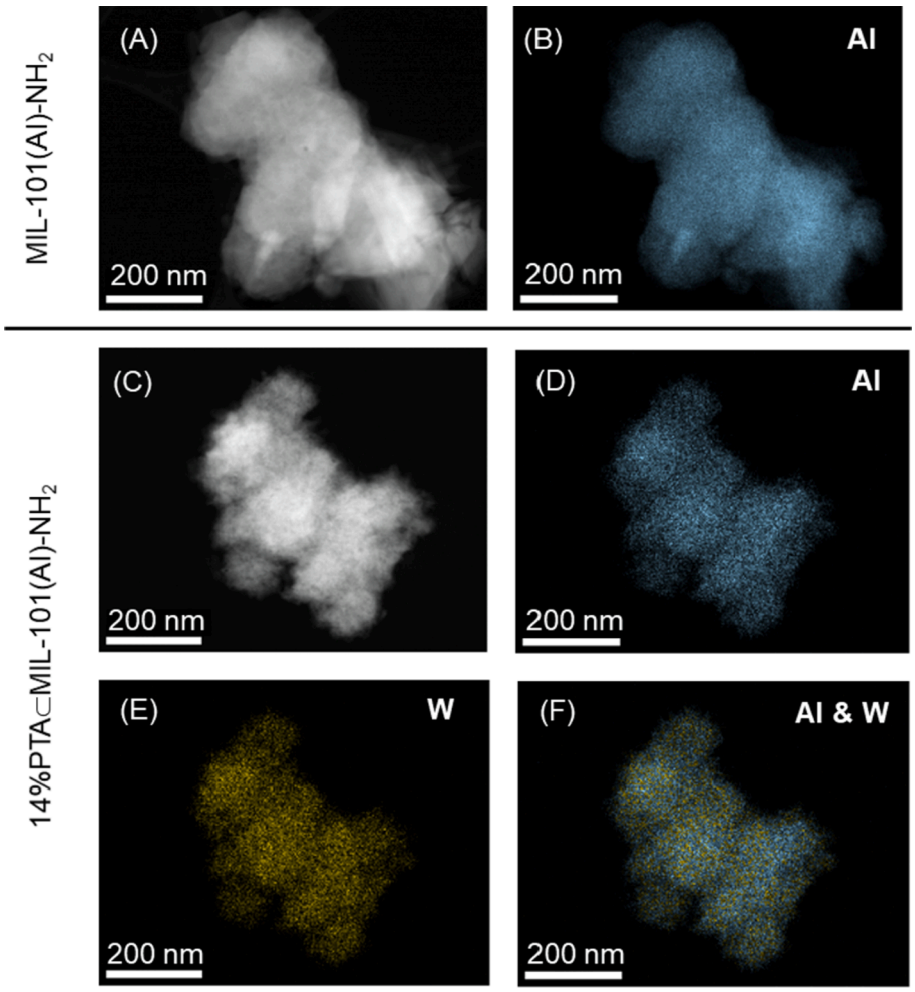

Fig. 1. STEM-HAADF images and corresponding elemental mapping of (A-B) MIL-101(Al)–NH_2 and (C-F) 14%PTA⊂MIL-101(Al)–NH_2.

FTIR was performed on catalysts (Fig. S4). The bare Al-MOF showed –NH_2 bands. The FTIR spectra of encapsulated PTA⊂Al-MOF catalysts contained bands from –NH_2 and W=O/W-O-W functionalities, which confirmed the encapsulation of PTA (*see Supplementary Materialss, Fig. S4*).

During synthesis, the PTA loading was varied from 0.1 to 2.0 g in 30 mL of DMF. To quantify the actual amount of encapsulated PTA, ICP-OES was conducted on encapsulated PTA⊂Al-MOF catalysts. As a control, the bare Al-MOF catalyst contained 11.56 wt.% Al, similar to a reported value [30]. All the encapsulated PTA⊂Al-MOF catalysts had a W/P molar ratio of 12, which was the same as that in PTA ($H_3PW_{12}O_{40}$) and which confirmed successful PTA encapsulation [82]. As expected, increases in PTA loading during synthesis progressively increased the W content and decreased the Al/W molar ratio. Interestingly, a PTA loading greater than 0.25 g/30 mL (entry 3) during synthesis did not result in a significant increase in encapsulated PTA. These results suggested that there was an optimal PTA loading that could occupy the MOF pores.

3.2. Acid properties of the catalysts by diffuse reflectance infrared Fourier transform spectroscopy

Selective glucose conversion to HMF requires a cooperative effect between Lewis and Brønsted acid catalysts for the cascade of glucose isomerization to fructose followed by fructose dehydration to HMF. Hence, it is important to distinguish and quantify the acid sites. To characterize the acid sites of the synthesized MOFs, DRIFTS was performed with adsorbed pyridine. Pyridine was chosen as an in-situ titrant for probing the acid site density of MOFs because of previous success in observation of Lewis acid and Brønsted acid sites in MOFs [83-85]. To avoid degradation of bare Al-MOF and encapsulated PTA⊂Al-MOF catalysts, DRIFTS was performed in a range of 30–150 °C according to their thermal stability from the TGA result (Fig. S5). After pyridine adsorption, the DRIFT spectra of these MOFs demonstrated characteristic bands at 1067, 1051, and 1030 cm^{-1} (Fig. 2). The 1067 and 1051 cm^{-1} bands corresponded to the interaction between pyridine and coordinated unsaturated metal sites (cus), i.e., Lewis acid sites [85,86]. The band at 1030 cm^{-1} corresponded to the interaction between pyridine and the Brønsted acid sites from encapsulated PTA. Surprisingly, a weak band at 1300 cm^{-1} in the MIL-101(Al)–NH_2 sample was observed, which suggested the presence of Brønsted acidity in MOFs. Similarly, studies by Herbst et al. [87], Halls et al. [88], Vimont et al. [89], and Volkringer et al.[85] showed that MIL-101(Cr), MIL-100(Cr), and MIL-100(Al) exhibited Brønsted acidity. The origin of Brønsted acidity in MOFs remains the topic of debate. However, its origin was hypothesized to come from the water molecules bound to metal sites [85]. Moreover, this water coordinated to the metal sites was not easily removed during activation of MOFs because a high temperature was required to remove the bound water. The high temperature can cause the structural damage to the MOFs and cause a loss in catalytic activity (*see Supplementary Materials and Fig. S6 for detail*).

Next, the Brønsted acid to Lewis acid ratio (B/L) was determined using the area integral of these bands (Table 1). An increase in encapsulated PTA loading increased the intensity of the Brønsted acid band at

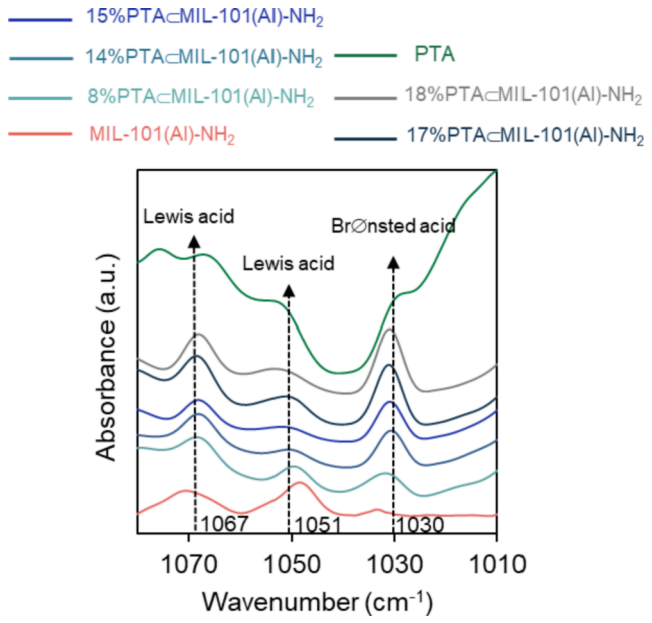

Fig. 2. Acid properties of encapsulated PTA⊂Al-MOF catalysts measured by diffuse reflectance infrared Fourier transform spectroscopy (DRIFTS).

1030 cm^{-1} and increased the B/L ratio of the catalysts. It should be noted that an increase in encapsulated PTA within MOFs was not proportional to an increase in B/L ratio. The acidic properties of encapsualted catalysts are difficult to be determined because the interaction between encapsulated species and the host support can modify their acidic properties. Juan-Alcañiz et al. showed the interaction between encapsualted PTA and the MIL-100(Cr) framework decreased Lewis acidity [90], which agrees with our finding of an increase in the B/L ratio after encapsulating more PTA becasuse of an increase in Brønsted acid sites and a decrease in Lewis acid sites.

3.3. PTA⊂MIL-101(Al)–NH_2-catalyzed glucose dehydration to 5-hydroxymethylfurfural

To determine the effect of PTA encapsulation on the catalytic performance, glucose dehydration was performed with encapsulated PTA⊂MIL-101(Al)–NH_2 catalysts (Fig. 3). A glucose:Al molar ratio of 25:1 was used in all experiments to normalize the Al content in the catalysts and compare catalytic performance with different encapsulated PTA loadings. As a control, a blank (no added catalyst) did not show any HMF production, which suggested that (1) the reaction was not autocatalytic, and (2) [C_4C_1im]Cl could not catalyze glucose dehydration. All catalysts were active for glucose dehydration in [C_4C_1im]Cl at 120 °C (Fig. 3A). Another control of using PTA as a catalyst showed a low HMF selectivity of 13% at 43% glucose conversion. Fructose, levulinic acid, or formic acid were not observed as products. These results suggested the PTA catalyst was not selective to HMF as in previous studies [52]. The bare Al-MOF catalyst appeared to be an efficient catalyst for glucose dehydration; however, it was not the most selective for HMF. All encapsulated PTA⊂Al-MOF catalysts were more selective for HMF than MIL-101(Al)–NH_2, which indicated that the encapsulated PTA in the pores of the Al-MOF enhanced HMF selectivity (Fig. S7). Moreover, HMF selectivity exhibited a volcano-shaped profile vs. the Brønsted to Lewis acid site ratio (B/L) (Fig. 4). The optimal B/L of 0.78 (14%PTA⊂Al-MOF catalyst) maximized the HMF selectivity of 58% at 44% glucose conversion at 120 °C after 2 h (Fig. 3B). These results suggested that cooperativity between Brønsted acidic PTA and Lewis acid sites of Al-MOF catalyst enhanced HMF selectivity.

To determine the importance of encapsulating PTA, a glucose dehydration reaction was performed with a physical mix of PTA and bare Al-MOF catalyst at the same composition as 14%PTA⊂Al-MOF catalyst. HMF selectivity by the physical mix catalyst was 33%, lower than that of encapsulated 14%PTA⊂Al-MOF catalysts (58%). These results confirmed the importance of PTA encapsulation in maximizing HMF selectivity. Interestingly, the HMF selectivity of the physically mixed catalyst converged to that of PTA alone (Fig. 3B). Although the Bronsted acid such as PTA catalyzes fructose dehydration to HMF, the free PTA molecules in the physical mix can catalyze aldol addition and condensation reactions from HMF via 2,5-dioxo-6-hydroxyhexanal [91], which resulted in humin formation. Moreover, the free PTA in the physical mix has a strong interaction with the surface of MOF, partially blocking the channels of MOFs and inhibiting the reactant accessibility to active sites [92,93]. This blocking effect is the reason why the HMF selectivity of the physical mix was lower than that of encapsulated PTA in MOFs [77]. Thus, the physical mix showed a high glucose conversion with a poor HMF selectivity, in agreement with the study by Zhang et al. [52].

To evaluate the stability of PTA in encapsulated PTA⊂MIL-101(Al)–NH_2 catalysts during the reaction, ICP-OES was performed on spent encapsulated 14%PTA⊂MIL-101(Al)–NH_2 catalyst (Fig. 3B). The W content of the encapsulated 14%PTA⊂MIL-101(Al)–NH_2 catalyst remained relatively constant (~11 wt.% W), which confirmed the stability of the PTA within the 14%PTA⊂MIL-101(Al)–NH_2 catalyst.

3.4. Solvent effect on the glucose dehydration to 5-hydroxymethylfurfural

The solvent affects the rate of reaction, product selectivity, and product stability [94,95]. A major consideration in catalytic biomass conversion is the stability of reactants, intermediates, and product in the reaction solvent. To investigate the effect of solvent on the stability of

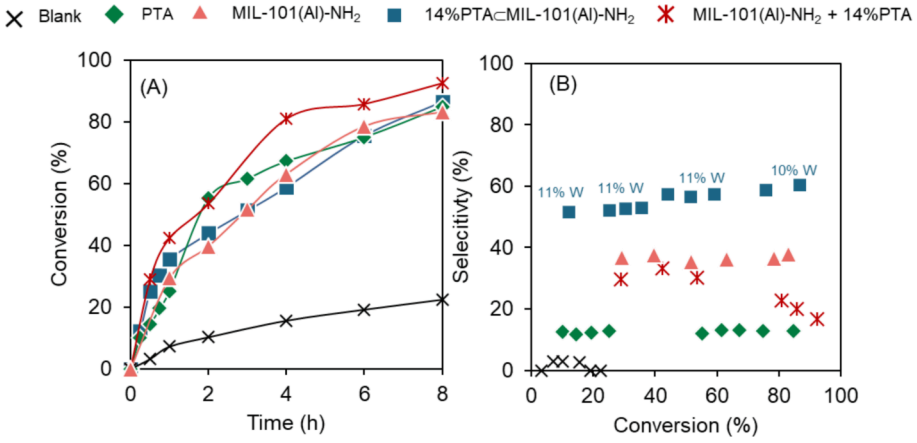

Fig. 3. Catalytic performance of encapsulated PTA⊂MIL-101(Al)–NH_2 catalysts. (A) Catalyst activity for glucose dehydration as a function of time. (B) HMF selectivity with the W content of the spent catalysts assessed by ICP-OES. Reaction condition: glucose:Al molar ratio = 25:1, 50 mg glucose, 1 g [C_4C_1im]Cl, 120 °C. Phosphotungstic acid (PTA) loading = 14 wt. % in PTA alone and physical mix (MIL-101(Al)–NH_2 + 14%PTA) to match the PTA in 14%PTA⊂Al-MOF. The percent of tungsten (%W) in Fig. 3B indicates the W content in the spent catalyst at the specific conversion.

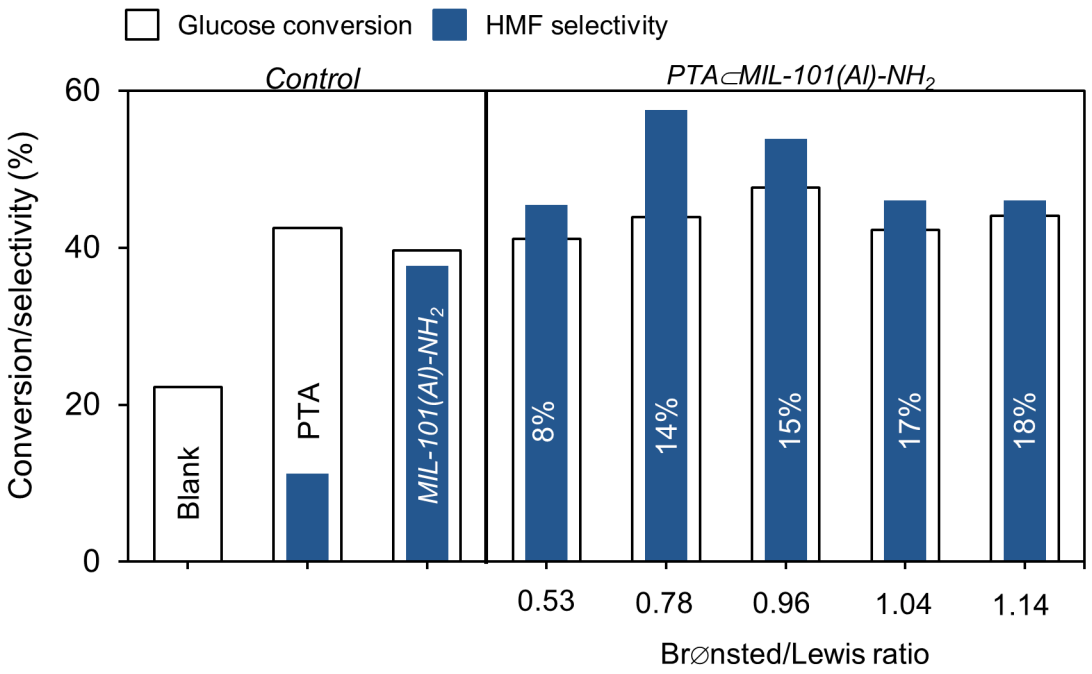

Fig. 4. HMF selectivity of encapsulated PTA⊂MIL-101(Al)–NH_2 catalysts at similar glucose conversions. Reaction condition: glucose:Al molar ratio = 25:1, 50 mg glucose, 1 g [C_4C_1im]Cl, 120 °C, 2 h. Numbers in the bar indicates wt.% of encapsulated PTA in PTA⊂MIL-101(Al)–NH_2.

these molecules, glucose, fructose and HMF were used as reactants in various solvents. The 14%PTA⊂Al-MOF was chosen as catalyst because it had the greatest HMF selectivity. For glucose, [C_4C_1im]Cl was the best performing solvent as shown by the greatest HMF selectivity at similar conversion to other solvents (Fig. 5). However, there was no obvious correlation between the HMF selectivity and solvent properties, such as dielectric constant or donor number.

Next, fructose was used as a reactant in [C_4C_1im]Cl (Fig. 6). Three solvents, DMA, 2-butanol, and *p*-dioxane, were selected for comparison with [C_4C_1im]Cl. Without added catalyst (blank), HMF selectivity was 47% at 96% fructose conversion in [C_4C_1im]Cl. The other solvents did not yield HMF and showed < 20% fructose conversion. As expected, added 14%PTA⊂MIL-101(Al)–NH_2 catalyst improved the HMF selectivity in all solvents; more specifically, HMF selectivity in [C_4C_1im]Cl was 89% at 94% fructose conversion, two times greater HMF selectivity compared with a reaction without added catalyst. Although added 14% PTA⊂MIL-101(Al)–NH_2 catalyst improved the fructose conversion in DMA, 2-butanol, and *p*-dioxane from < 20% to greater than 60%, the HMF selectivity in these three solvents was low (< 22%). These results suggested that [C_4C_1im]Cl can act as both acid catalyst [96,97] and solvent in fructose dehydration reaction. Moreover, the 14%PTA⊂MIL-101(Al)–NH_2 enhanced HMF selectivity from fructose dehydration.

Next, HMF was used as a reactant in these four solvents to investigate the HMF stability (Fig. 7). Without any catalyst (blank), HMF conversion was 11% in [C_4C_1im]Cl, and conversion increased slightly in other solvents. There were no identifiable products, which suggested the HMF was likely degraded into humin [98,99]. The added 14%PTA⊂MIL-101(Al)–NH_2 catalyst enhanced HMF conversion to 15% in [C_4C_1im]Cl. The presence of 14%PTA⊂MIL-101(Al)–NH_2 catalyst in other solvents improved the HMF conversion more than in [C_4C_1im]Cl. These results suggested that (1) HMF was not stable in these solvents and (2) although the 14%PTA⊂MIL-101(Al)–NH_2 catalyst improved glucose/fructose

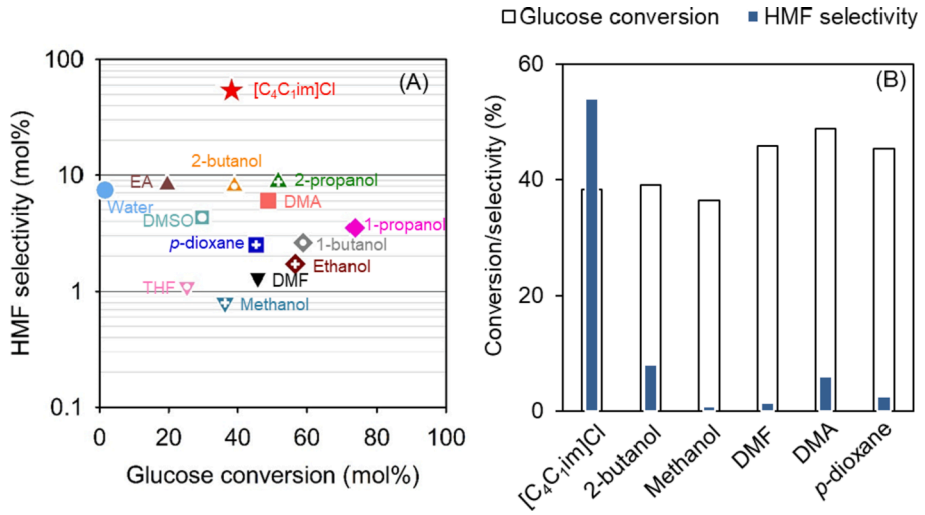

Fig. 5. Solvent effect on glucose conversion and HMF selectivity (A) and comparison of conversion and selectivity in selected solvents (B) by 14%PTA⊂MIL-101(Al)–NH_2 catalyst. Reaction condition: glucose:Al molar ratio = 25:1, 50 mg glucose, 1 g solvent, 120 °C, 2 h.

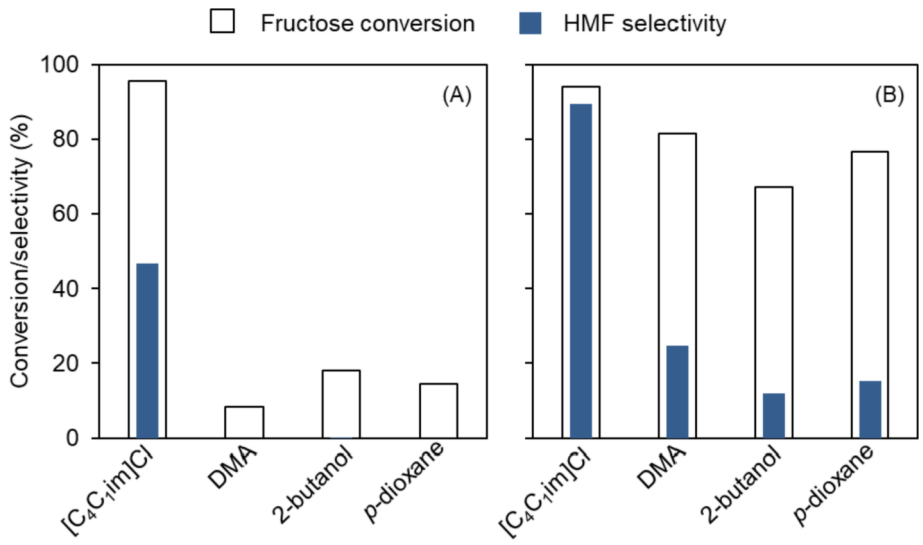

Fig. 6. Solvent effect on fructose conversion to HMF (A) without added catalyst, and (B) catalytic performance of encapsulated 14%PTA⊂MIL-101(Al)–NH_2. Reaction condition: fructose:Al molar ratio = 25:1, 50 mg fructose, 1 g solvent, 120 °C, 2 h.

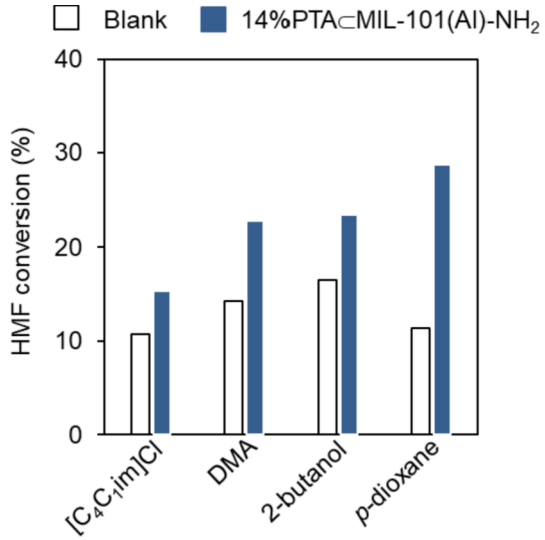

Fig. 7. HMF conversion in different solvents with/without 14%PTA⊂MIL-101(Al)–NH_2. Reaction condition: HMF:Al molar ratio = 25:1, 50 mg HMF, 1 g solvent, 120 °C, 2 h.

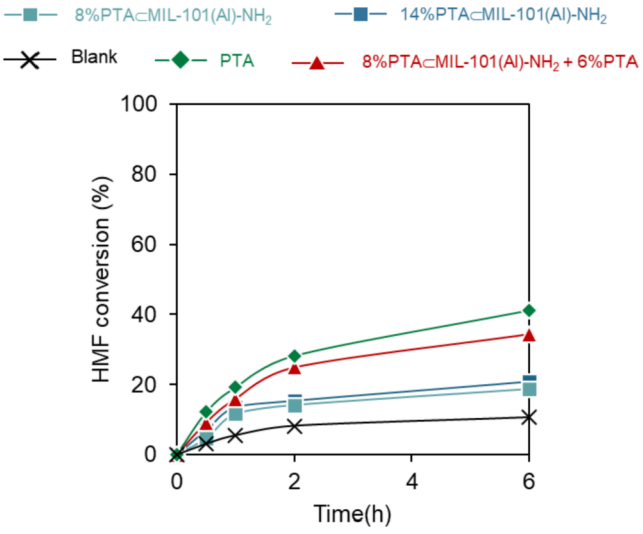

Fig. 8. HMF conversion by encapsulated PTA⊂MIL-101(Al)–NH_2. Reaction condition: 50 mg HMF, 30 mg catalyst, 1 g [C_4C_1im]Cl, 120 °C. Phosphotungstic acid loading = 14 wt.% in PTA alone (green) and physical mix between 8%PTA⊂MIL-101(Al)–NH_2 + 6%PTA (red) to match the PTA loading in 14% PTA⊂Al-MOF (dark blue).

dehydration to HMF, the catalyst facilitated HMF conversion to humin. Thus, to minimize HMF degradation and maintain the high HMF yield, a reactive HMF extraction process should be considered [100].

3.5. Stability of HMF in the catalytic system and [C_4C_1im]Cl

To maintain the high HMF selectivity in the reaction, it was important to determine the stability of the HMF under the reaction condition. Thus, HMF was heated in the same experimental condition that was used for glucose dehydration (120 °C) in [C_4C_1im]Cl solvent and catalysts. Without catalysts (blank), HMF degradation was ~ 11% after 6 h (Fig. 8). Levulinic acid and formic acid were not observed. These results suggested that [C_4C_1im]Cl was not able to rehydrate HMF. With added encapsulated 8% and 14%PTA⊂Al-MOF catalysts, a slight increase in HMF conversion was observed, which reached ~ 18% after 6 h. With PTA alone, the HMF conversion rate was 41%, greater than that of conversion in the presence of encapsulated 8% and 14%PTA⊂Al-MOF catalysts and reaching 19% and 21% after 6 h, respectively.

Next, the physical mixture of PTA and 8%PTA⊂MIL-101(Al)–NH_2 catalyst was evaluated to check the HMF stability. The amount of PTA in the physical mixture of PTA and 8%PTA⊂Al-MOF catalyst was maintained at the same level as for the encapsulated 14%PTA⊂Al-MOF catalyst. As expected, the physical mixture increased HMF conversion by 34% at 6 h reaction time compared with 21% HMF conversion by 14% PTA⊂Al-MOF catalyst. These results demonstrated that PTA in the bulk solution degraded the HMF and decreased the HMF selectivity, similar to a finding of Zhang et al. [52]. The encapsulation of PTA in the pores of Al-MOF catalyst minimized PTA leaching into the solvent and limited conversion of HMF, which, in turn, maintained the HMF selectivity.

3.6. Reuse of encapsulated PTA⊂MIL-101(Al)–NH_2 for glucose dehydration

To determine the ability to reuse the encapsulated PTA⊂Al-MOF catalyst, the spent catalyst was recovered by centrifugation, washed

with water, and dried in a vacuum oven at 130 °C to remove moisture, residual products, intermediates, and unreacted glucose. Then, the catalyst was reused four times. The 14%PTA⊂Al-MOF was chosen because it had the greatest HMF selectivity. The 14%PTA⊂Al-MOF catalyst maintained its catalytic performance with HMF selectivity of ~ 55% at 40% glucose conversion after the 4th cycle, < 10% decrease in both glucose conversion and HMF selectivity compared with fresh catalyst (Fig. 9). In all cycles, the selectivity to HMF was between 55 and 62%. Next, ICP-EOS was used to measure the Tungsten (W) content in the spent catalysts. Only a slight W loss (< 3 wt.%) in the spent catalysts was observed after four recycles, which indicated that little to no PTA leached from the 14%PTA⊂Al-MOF catalyst.

3.7. Proposed chemical pathway for glucose dehydration to HMF by PTA⊂MIL-101(Al)–NH_2

On the basis of the foregoing findings, Scheme 2 shows a proposed mechanism for glucose dehydration to HMF by PTA⊂MIL-101(Al)–NH_2 catalysts. The reaction proceeds by the synergy between Lewis-Brønsted acid sites: (1) glucose isomerization to fructose by the Lewis acid of MIL-101(Al)–NH_2, and (2) dehydration of resulting fructose to HMF by the Brønsted acid of PTA and/or MIL-101(Al)–NH_2.

The glucose isomerization to fructose by Lewis acid sites consists of a sequence of ring opening, deprotonation, isomerization, protonation, and ring closure processes as shown by Hensen et al. [101-103]. We postulated that glucose initially binds to the Al active site imbedded in the MIL-101 framework via its ring oxygen atom and followed by the ring opening process to form the acyclic glucose. Subsequently, the deprotonation of the hydroxyl group at C_2 occurred by the metal-oxo clusters. Next, the aldose-ketose isomerization induces the hydride shift from the C_2 to C_1 carbon atom. The reaction undergoes a ring-closure reaction yielding anionic fructofuranose bound to Al site. Finally, the terminal oxygen anionic fructofuranose is protonated to generate fructose.

The fructose undergoes dehydration by Brønsted acid sites to produce HMF by dehydration and tautomerization. First, the hydroxyl group of the fructose at the alpha position is protonated by acidic protons of Brønsted acid catalysts, which resulted in the formation of water. Next, the cyclic enol intermediate is formed and subsequently tautomerized to 2,5-anhydro-D-mannose [104-106]. Then, the reaction proceeds by two sequential dehydrations to form HMF.

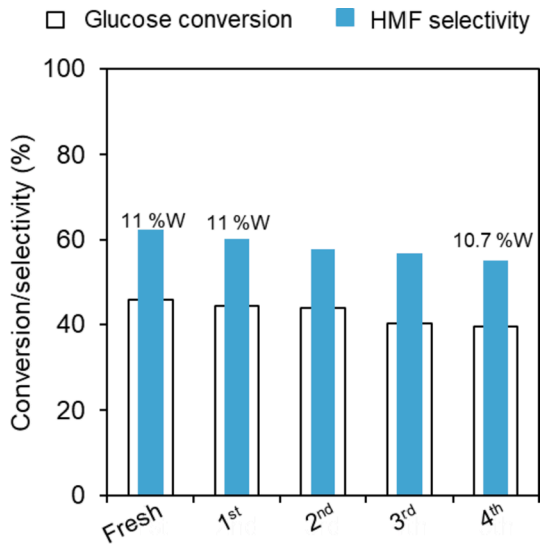

Fig. 9. Reuse of 14%PTA⊂MIL-101(Al)–NH_2 for glucose dehydration. Reaction condition: glucose: Al molar ratio = 25:1, 1 g [C_4C_1im]Cl, 120 °C, 2 h. Tungsten content (%W) indicates the W content in the spent catalyst.

4. Discussion

A major challenge in selective glucose conversion to HMF is the design of catalysts that possess Lewis and Bronsted acid sites that can act cooperatively [15,107,108]. Here, the effect of PTA encapsulation in PTA⊂MIL-101(Al)–NH_2 catalysts (PTA⊂Al-MOF) on glucose conversion to HMF was investigated. The synergy between encapsulated PTA and Al-MOFs enabled the high HMF selectivity. Moreover, the results demonstrated that the encapsulation of PTA in MIL-101(Al)–NH_2 catalysts minimized PTA leaching into the bulk solution, thereby preventing degradation of the HMF product.

The most significant finding was that the HMF selectivity strongly depended on the location of the PTA. Encapsulation of PTA in MIL-101 (Al)–NH_2 pores provided two benefits. First, the close proximity between the Lewis acid sites of the Al-MOF and the Brønsted acidic PTA promoted HMF formation. The fructose formed from glucose isomerization by Lewis acid (MIL-101(Al)–NH_2) was dehydrated to HMF by the encapsulated PTA catalyst. Tangsermvit et al. showed that the proximity between Lewis and Brønsted acid sites was important in achieving a high HMF yield [109], a result that agrees with our findings. Second, encapsulated PTA catalysts minimized PTA leaching into the bulk solution and, consequently, prevented HMF degradation. Although Brønsted acids catalyze fructose dehydration to HMF, they also catalyze undesired HMF rehydration to levulinic acid [110] and/or degradation to humin [11]. The MIL-101 structure of the Al-MOF possesses both mesoporous windows (29–34 Å) and microporous windows, the latter corresponding to large hexagonal pores (15–16 Å), and somewhat smaller pentagonal pores (~12 Å) [111-113]. Keggin-type heteropolyacids, ~13–14 Å in size [53], are larger than the pentagonal pores in MIL-101, thereby preventing heteropolyacids from leaching out and causing side reactions (rehydration and/or humin formation). These results explained the retention of HMF selectivity and the ability to recycle the PTA⊂MIL-101(Al)–NH_2 catalyst. Hence, encapsulated Brønsted acidic PTA in the pores of MIL-101(Al)–NH_2 not only provided Brønsted acidity for fructose dehydration but also prevented PTA leaching into the bulk solution, that otherwise had the potential to degrade HMF.

Another significant finding was the discovery of the high selectivity of PTA⊂Al-MOF for glucose dehydration. Many investigators used solid Lewis acid catalysts (Sn-containing β-zeolites [20] and Nb_2O_5 [18]) with homogeneous catalysts such as HCl to maximize HMF selectivity (Table S3). Their results suggested that the cooperative effect between Lewis acid and Brønsted acid species was critical in maximizing HMF selectivity in glucose dehydration. Qu et al. impregnated SO_4^{2-} on ZrO_2 by H_2SO_4 acid [114]. Although the SO_4^{2-}/ZrO_2 in biphasic THF/H_2O system reached a high HMF selectivity of 67% at 93% glucose conversion, both HMF selectivity and glucose conversion dropped ~ 10% after the 4th catalyst recycling due to leaching of SO_4^{2-} [114]. The ability to create the solid bifunctional Lewis-Bronsted catalysts will enhance the commercial feasibility of HMF production. Zhang et al. encapsulated PTA in MIL-101(Cr) to produce the bifunctional acid catalysts with PTA as a Brønsted acid and MIL-101(Cr) as a Lewis acid [52]. The PTA⊂MIL-101(Cr) catalysts were selective toward HMF in fructose dehydration. However, they were not selective toward HMF in glucose dehydration and gave only 10% HMF selectivity at 21% glucose conversion at 100 °C after 3 h. Compared with MOF-derived catalysts for glucose dehydration, the PTA⊂Al-MOF catalysts described in this report were superior to other MOF-derived catalysts in terms of HMF selectivity (Table S3).

These findings demonstrate that PTA⊂Al-MOF catalyst was a selective and recyclable catalyst for glucose dehydration to HMF. The PTA⊂MIL-101(Al)–NH_2 catalyst was easy to synthesize compared with other solid acid catalysts for selective glucose conversion to HMF, such as modified β-zeolites [115]. Moreover, the ability to control the ratio of numbers of Brønsted acid sites to Lewis acid sites in PTA⊂Al-MOF catalysts provides opportunities to use the catalysts in various organic reactions, such as esterification [116], alkylation [117], and benzylation

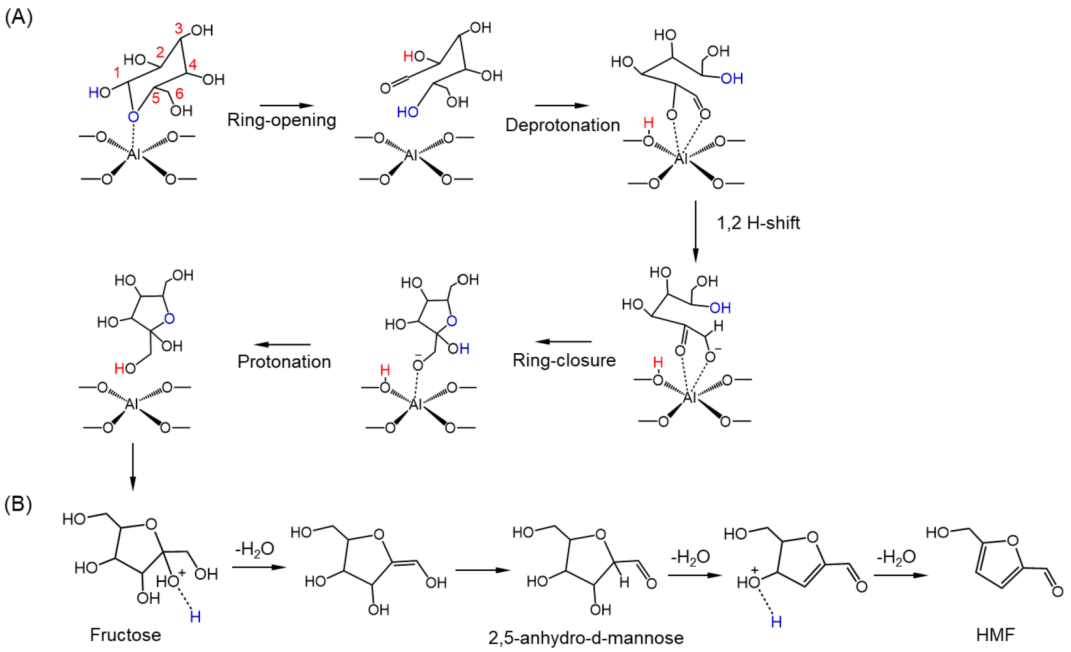

Scheme 2. Proposed reaction mechanism for glucose dehydration to HMF over PTA⊂MIL-101(Al)–NH_2. The reaction proceeds by (A) glucose dehydration to fructose, followed by (B) fructose dehydration to HMF.

[118].

Although PTA⊂Al-MOF catalyst is promising for selective glucose conversion to HMF, the interactions between the framework, metal nodes, and PTA (acidic protons) that affect the acid properties and catalytic performance has not been extensively investigated. Juan-Alcañiz et al. reported the partial W substitution by Cr^{3+} of MIL-101(Cr) at high temperatures [53]. The W-substituted heteropolyacids and/or the formation of W-Al complex metal nodes might be the active sites for this reaction. Additional studies should identify the interaction between W in PTA and Al in Al-MOF by ^{27}Al Magic Angle Spin (MAS) Nuclear Magnetic Resonance (NMR). The knowledge will help in designing selective catalysts and systems for glucose dehydration.

5. Conclusion

Phosphotungstic acid encapsulated MIL-101(Al)–NH_2 catalyst (PTA⊂MIL-101(Al)–NH_2) was developed for selective glucose conversion to HMF. The encapsulation of Brønsted acidic phosphotungstic acid in the pores of MIL-101(Al)–NH_2 provided the proximity between Brønsted acid sites and Lewis acid sites of MIL-101(Al)–NH_2 for the efficient cascade of glucose isomerization and fructose dehydration. The synergistic effect of Brønsted and Lewis acid sites in the phosphotungstic acid encapsulated MIL-101(Al)–NH_2 catalyst is the key contributor to the high HMF selectivity and glucose conversion; this synergy cannot occur if the agents are introduced separately. Moreover, the encapsulated phosphotungstic acid was stable in the pores of MIL-101(Al)–NH_2, which minimized leaching of PTA into the bulk solution and reaction with the HMF to generate undesired products. As a result, the encapsulated PTA⊂MIL-101(Al)–NH_2 catalyst maintained its catalytic performance after recycling four times. These results underscore the importance of phosphotungstic acid encapsulation to provide the cooperative effect between Brønsted and Lewis acidic sites for maximizing the HMF formation and minimizing subsequent HMF conversion/degradation. This encapsulated metal–organic framework catalyst should be applicable to other acid-catalyzed biomass transformations.

CRediT authorship contribution statement

Mohammad Shahinur Rahaman: Conceptualization, Methodology, Investigation, Writing – original draft, Writing – review & editing. **Sarttrawut Tulaphol:** Conceptualization, Validation, Formal analysis, Writing – review & editing, Visualization. **Md Anwar Hossain:** Methodology, Investigation, Writing – original draft. **Jacek B. Jasinski:** Investigation, Writing – original draft. **Ning Sun:** Writing – review & editing, Supervision. **Anthe George:** Writing – review & editing, Supervision. **Blake A. Simmons:** Writing – review & editing, Supervision. **Thana Maihom:** Formal analysis, Writing – review & editing. **Mark Crocker:** Writing – review & editing, Supervision. **Noppadon Sathitsuksanoh:** Conceptualization, Methodology, Validation, Visualization, Supervision, Project administration, Writing – review & editing, Funding acquisition.

Declaration of Competing Interest

The authors declare that they have no known competing financial interests or personal relationships that could have appeared to influence the work reported in this paper.

Acknowledgment

A part of this material is based upon work supported by the National Science Foundation under Cooperative Agreement No. 1355438 and Internal Research Grant, Office of the Executive Vice President for Research, University of Louisville. This work was performed in part at the Conn Center for Renewable Energy Research at the University of Louisville, which belongs to the National Science Foundation NNCI KY Manufacturing and Nano Integration Node, supported by ECCS-1542174. The authors would like to thank Dr. Howard Fried for his valuable comments and suggestions on the manuscript.

Appendix A. Supplementary data

Supplementary data to this article can be found online at https://doi.org/10.1016/j.fuel.2021.122459.

References

[1] Regnier E. Oil and energy price volatility. Energy Econ 2007;29(3):405–27.

[2] Awodumi OB, Adewuyi AO. The role of non-renewable energy consumption in economic growth and carbon emission: Evidence from oil producing economies in Africa. Energy Strategy Rev 2020;27:100434. https://doi.org/10.1016/j.esr.2019.100434.

[3] Kuster BFM. 5-Hydroxymethylfurfural (HMF). A review focussing on its manufacture. Starch-Stärke 1990;42(8):314–21.

[4] Fan C, Guan H, Zhang H, Wang J, Wang S, Wang X. Conversion of fructose and glucose into 5-hydroxymethylfurfural catalyzed by a solid heteropolyacid salt. Biomass Bioenergy 2011;35(7):2659–65.

[5] Yong G, Zhang Y, Ying J. Efficient catalytic system for the selective production of 5-hydroxymethylfurfural from glucose and fructose. Angew Chem Int Ed 2008;47(48):9345–8.

[6] Xu H, Wang Z, Huang J, Jiang Y. Thermal Catalytic Conversion of Biomass-Derived Glucose to Fine Chemicals. Energy Fuels 2021;35(10):8602–16.

[7] Wrigstedt P, Keskiväli J, Leskelä M, Repo T. The Role of Salts and Brønsted Acids in Lewis Acid-Catalyzed Aqueous-Phase Glucose Dehydration to 5-Hydroxymethylfurfural. ChemCatChem 2015;7(3):501–7.

[8] Yang L, Tsilomelekis G, Caratzoulas S, Vlachos DG. Mechanism of Brønsted Acid-Catalyzed Glucose Dehydration. ChemSusChem 2015;8(8):1334–41.

[9] vanPutten R-J, Soetedjo JNM, Pidko EA, van der Waal JC, Hensen EJM, deJong Ed, et al. Dehydration of different ketoses and aldoses to 5-hydroxymethylfurfural. ChemSusChem 2013;6(9):1681–7.

[10] Ordomsky VV, Sushkevich VL, Schouten JC, van der Schaaf J, Nijhuis TA. Glucose dehydration to 5-hydroxymethylfurfural over phosphate catalysts. J Catal 2013;300:37–46.

[11] Shen J, Wyman CE. Hydrochloric acid-catalyzed levulinic acid formation from cellulose: data and kinetic model to maximize yields. AIChE J 2012;58(1):236–46.

[12] Caratzoulas S, Davis ME, Gorte RJ, Gounder R, Lobo RF, Nikolakis V, et al. Challenges of and insights into acid-catalyzed transformations of sugars. J Phys Chem C 2014;118(40):22815–33.

[13] Kruger JS, Nikolakis V, Vlachos DG. Aqueous-phase fructose dehydration using Brønsted acid zeolites: Catalytic activity of dissolved aluminosilicate species. Appl Catal, A 2014;469:116–23.

[14] Román-Leshkov Y, Moliner M, Labinger JA, Davis ME. Mechanism of glucose isomerization using a solid Lewis acid catalyst in water. Angew Chem Int Ed 2010;49(47):8954–7.

[15] Pagán-Torres YJ, Wang T, Gallo JMR, Shanks BH, Dumesic JA. Production of 5-hydroxymethylfurfural from glucose using a combination of Lewis and Brønsted acid catalysts in water in a biphasic reactor with an alkylphenol solvent. ACS Catal 2012;2(6):930–4.

[16] Chen SS, Maneerung T, Tsang DCW, Ok YS, Wang C-H. Valorization of biomass to hydroxymethylfurfural, levulinic acid, and fatty acid methyl ester by heterogeneous catalysts. Chem Eng J 2017;328:246–73.

[17] Bounoukta CE, Megías-Sayago C, Ammari F, Ivanova S, Monzon A, Centeno MA, et al. Dehydration of glucose to 5-hydroxymethlyfurfural on bifunctional carbon catalysts. Appl Catal, B 2021;286:119938. https://doi.org/10.1016/j.apcatb.2021.119938.

[18] Vieira JL, Almeida-Trapp M, Mithöfer A, Plass W, Gallo JMR. Rationalizing the conversion of glucose and xylose catalyzed by a combination of Lewis and Brønsted acids. Catal Today 2020;344:92–101.

[19] Swift TD, Nguyen H, Anderko A, Nikolakis V, Vlachos DG. Tandem Lewis/Brønsted homogeneous acid catalysis: conversion of glucose to 5-hydoxymethylfurfural in an aqueous chromium (III) chloride and hydrochloric acid solution. Green Chem 2015;17(10):4725–35.

[20] Nikolla E, Román-Leshkov Y, Moliner M, Davis ME. "One-pot" synthesis of 5-(hydroxymethyl) furfural from carbohydrates using tin-beta zeolite. ACS Catal 2011;1(4):408–10.

[21] Cole-Hamilton DJ. Homogeneous catalysis–new approaches to catalyst separation, recovery, and recycling. Science 2003;299(5613):1702–6.

[22] Farrusseng D, Aguado S, Pinel C. Metal–organic frameworks: opportunities for catalysis. Angew Chem Int Ed 2009;48(41):7502–13.

[23] Lee J, Farha OK, Roberts J, Scheidt KA, Nguyen ST, Hupp JT. Metal–organic framework materials as catalysts. Chem Soc Rev 2009;38(5):1450–9.

[24] Férey G. Hybrid porous solids: past, present, future. Chem Soc Rev 2008;37(1):191–214.

[25] Li H, Eddaoudi M, O'Keeffe M, Yaghi OM. Design and synthesis of an exceptionally stable and highly porous metal-organic framework. Nature 1999;402(6759):276–9.

[26] Kitagawa S, Kitaura R, Noro S-I. Functional porous coordination polymers. Angew Chem Int Ed 2004;43(18):2334–75.

[27] Dhakshinamoorthy A, Alvaro M, Garcia H. Commercial metal–organic frameworks as heterogeneous catalysts. Chem Commun 2012;48(92):11275–88.

[28] Chen Y-Z, Zhou Y-X, Wang H, Lu J, Uchida T, Xu Q, et al. Multifunctional PdAg@MIL-101 for one-pot cascade reactions: combination of host–guest cooperation and bimetallic synergy in catalysis. ACS Catal 2015;5(4):2062–9.

[29] Henschel A, Gedrich K, Kraehnert R, Kaskel S. Catalytic properties of MIL-101. Chem Commun 2008;35:4192–4.

[30] Bromberg L, Su X, Hatton TA. Heteropolyacid-functionalized aluminum 2-aminoterephthalate metal-organic frameworks as reactive aldehyde sorbents and catalysts. ACS Appl Mater Interfaces 2013;5(12):5468–77.

[31] Toyao T, Fujiwaki M, Horiuchi Y, Matsuoka M. Application of an amino-functionalised metal–organic framework: An approach to a one-pot acid–base reaction. Rsc Adv 2013;3(44):21582–7.

[32] Serra-Crespo P, Ramos-Fernandez EV, Gascon J, Kapteijn F. Synthesis and characterization of an amino functionalized MIL-101 (Al): separation and catalytic properties. Chem Mater 2011;23(10):2565–72.

[33] Srirambalaji R, Hong S, Natarajan R, Yoon M, Hota R, Kim Y, et al. Tandem catalysis with a bifunctional site-isolated Lewis acid–Brønsted base metal–organic framework, NH2-MIL-101(Al). Chem Commun 2012;48(95):11650. https://doi.org/10.1039/c2cc36678a.

[34] Ramos-Fernandez EV, Pieters C, van der Linden B, Juan-Alcañiz J, Serra-Crespo P, Verhoeven MWGM, et al. Highly dispersed platinum in metal organic framework NH_2-MIL-101 (Al) containing phosphotungstic acid–Characterization and catalytic performance. J Catal 2012;289:42–52.

[35] Ma L, Abney C, Lin W. Enantioselective catalysis with homochiral metal–organic frameworks. Chem Soc Rev 2009;38(5):1248–56.

[36] Corma A, García H, Llabrés i Xamena FX. Llabrés i Xamena FX. Engineering metal organic frameworks for heterogeneous catalysis. Chem Rev 2010;110(8):4606–55.

[37] Yoon M, Srirambalaji R, Kim K. Homochiral metal–organic frameworks for asymmetric heterogeneous catalysis. Chem Rev 2012;112(2):1196–231.

[38] Jiang J, Yaghi OM. Brønsted acidity in metal–organic frameworks. Chem Rev 2015;115(14):6966–97.

[39] Horn MR, Singh A, Alomari S, Goberna-Ferrón S, Benages-Vilau R, Chodankar N, et al. Polyoxometalates (POMs): from electroactive clusters to energy materials. Energy Environ Sci 2021;14(4):1652–700.

[40] Gumerova NI, Rompel A. Synthesis, structures and applications of electron-rich polyoxometalates. Nat Rev Chem 2018;2(2):0112.

[41] Kazanskij LP, Spitsyn VI. Proton-acceptor capacity and energy of oxygen 1s-electrons of heteropolyanions. Dokl Akad Nauk SSSR 1976;227(1):140–3.

[42] Misono M. Recent progress in the practical applications of heteropolyacid and perovskite catalysts: Catalytic technology for the sustainable society. Catal Today 2009;144(3-4):285–91.

[43] Wang S-S, Yang G-Y. Recent advances in polyoxometalate-catalyzed reactions. Chem Rev 2015;115(11):4893–962.

[44] Deng W, Zhang Q, Wang Y. Polyoxometalates as efficient catalysts for transformations of cellulose into platform chemicals. Dalton Trans 2012;41(33):9817–31.

[45] Weinstock IA, Schreiber RE, Neumann R. Dioxygen in polyoxometalate mediated reactions. Chem Rev 2018;118(5):2680–717.

[46] Enferadi-Kerenkan A, Do T-O, Kaliaguine S. Heterogeneous catalysis by tungsten-based heteropoly compounds. Catal Sci Technol 2018;8(9):2257–84.

[47] Zhong J, Pérez-Ramírez J, Yan N. Biomass valorisation over polyoxometalate-based catalysts. Green Chem 2021;23(1):18–36.

[48] Wang C, Zhang L, Zhou T, Chen J, Xu F. Synergy of Lewis and Brønsted acids on catalytic hydrothermal decomposition of carbohydrates and corncob acid hydrolysis residues to 5-hydroxymethylfurfural. Sci Rep 2017;7:40908.

[49] Wang Z, Chen Q. Conversion of 5-hydroxymethylfurfural into 5-ethoxymethylfurfural and ethyl levulinate catalyzed by MOF-based heteropolyacid materials. Green Chem 2016;18(21):5884–9.

[50] Zhan G, Zeng HC. Integrated nanocatalysts with mesoporous silica/silicate and microporous MOF materials. Coord Chem Rev 2016;320-321:181–92.

[51] Liang D-D, Liu S-X, Ma F-J, Wei F, Chen Y-G. A crystalline catalyst based on a porous metal-organic framework and 12-tungstosilicic acid: Particle size control by hydrothermal synthesis for the formation of dimethyl ether. Adv Synth Catal 2011;353(5):733–42.

[52] Zhang Y, Degirmenci V, Li C, Hensen EJM. Phosphotungstic acid encapsulated in metal–organic framework as catalysts for carbohydrate dehydration to 5-hydroxymethylfurfural. ChemSusChem 2011;4(1):59–64.

[53] Juan-Alcañiz J, Ramos-Fernandez EV, Lafont U, Gascon J, Kapteijn F. Building MOF bottles around phosphotungstic acid ships: One-pot synthesis of bi-functional polyoxometalate-MIL-101 catalysts. J Catal 2010;269(1):229–41.

[54] Sun M, Chen W-C, Zhao L, Wang X-L, Su Z-M. A PTA@MIL-101(Cr)-diatomite composite as catalyst for efficient oxidative desulfurization. Inorg Chem Commun 2018;87:30–5.

[55] Maksimchuk NV, Kovalenko KA, Arzumanov SS, Chesalov YA, Melgunov MS, Stepanov AG, et al. Hybrid polyoxotungstate/MIL-101 materials: synthesis, characterization, and catalysis of H_2O_2-based alkene epoxidation. Inorg Chem 2010;49(6):2920–30.

[56] Su Ye, Chang G, Zhang Z, Xing H, Su B, Yang Q, et al. Catalytic dehydration of glucose to 5-hydroxymethylfurfural with a bifunctional metal-organic framework. AIChE J 2016;62(12):4403–17.

[57] Das AP, Mishra S. Hexavalent chromium (VI): Environment pollutant and health hazard. J Environ Res Dev 2008;2(3):386–92.

[58] Tulaphol S, Hossain MA, Rahaman MS, Liu L-Y, Phung TK, Renneckar S, et al. Direct production of levulinic acid in one pot from hemp hurd by dilute acid in ionic liquids. Energy Fuels 2020;34(2):1764–72.

[59] Sun N, Liu H, Sathitsuksanoh N, Stavila V, Sawant M, Bonito A, et al. Production and extraction of sugars from switchgrass hydrolyzed in ionic liquids. Biotechnol Biofuels 2013;6(1). https://doi.org/10.1186/1754-6834-6-39.

[60] Groff D, George A, Sun N, Sathitsuksanoh N, Bokinsky G, Simmons BA, et al. Acid enhanced ionic liquid pretreatment of biomass. Green Chem 2013;15(5):1264. https://doi.org/10.1039/c3gc37086k.

[61] Kozhevnikov IV. Advances in catalysis by heteropolyacids. Russ Chem Rev 1987;56(9):811–25.

[62] Haul R. SJ Gregg, KSW Sing: adsorption, surface area and porosity. 2. auflage, academic press, London 1982. 303 Seiten, Preis: $49.50. Wiley Online Library; 1982.

[63] Sing KSW. Reporting physisorption data for gas/solid systems with special reference to the determination of surface area and porosity (Recommendations 1984). Pure Appl Chem 1985;57(4):603–19.

[64] Jaroniec M, Kruk M, Sayari A. Adsorption methods for characterization of surface and structural properties of mesoporous molecular sieves. Stud Surf Sci Catal: Elsevier 1998:325–32.

[65] Dollimore D, Spooner P, Turner A. The BET method of analysis of gas adsorption data and its relevance to the calculation of surface areas. Surf Technol 1976;4(2):121–60.

[66] Barrett EP, Joyner LG, Halenda pp.. The determination of pore volume and area distributions in porous substances. I. Computations from nitrogen isotherms. J Am Chem Soc 1951;73(1):373–80.

[67] Xu J, Liu J, Li Z, Wang X, Wang Z. Synthesis, structure and properties of Pd@MOF-808. J Mater Sci 2019;54(19):12911–24.

[68] Jana SK, Nishida R, Shindo K, Kugita T, Namba S. Pore size control of mesoporous molecular sieves using different organic auxiliary chemicals. Microporous Mesoporous Mater 2004;68(1-3):133–42.

[69] Groen JC, Peffer LAA, Pérez-Ramírez J. Pore size determination in modified micro-and mesoporous materials. Pitfalls and limitations in gas adsorption data analysis. Microporous Mesoporous Mater 2003;60(1-3):1–17.

[70] Osman AI, Abu-Dahrieh JK, Rooney DW, Halawy SA, Mohamed MA, Abdelkader A. Effect of precursor on the performance of alumina for the dehydration of methanol to dimethyl ether. Appl Catal, B 2012;127:307–15.

[71] Santos KMA, Albuquerque EM, Innocenti G, Borges LEP, Sievers C, Fraga MA. The role of Brønsted and water-tolerant Lewis acid sites in the cascade aqueous-phase reaction of triose to lactic acid. ChemCatChem 2019;11(13):3054–63.

[72] Yu D, Wu M, Hu Q, Wang L, Lv C, Zhang L. Iron-based metal-organic frameworks as novel platforms for catalytic ozonation of organic pollutant: Efficiency and mechanism. J Hazard Mater 2019;367:456–64.

[73] Li S-W, Wang W, Zhao J-S. Effective and reusable oxidative desulfurization of dibenzothiophene via magnetic amino-MIL-101 supported $H_3PMo_6W_6O_{40}$ components: comparison influence on various types of MIL-101. Energy Fuels 2020;34(4):4837–48.

[74] Qin L, Li Z, Hu Q, Xu Z, Guo X, Zhang G. One-pot assembly of metal/organic-acid sites on amine-functionalized ligands of MOFs for photocatalytic hydrogen peroxide splitting. Chem Commun 2016;52(44):7110–3.

[75] Wang J, Liu Y, Guo X, Qu H, Chang R, Ma J. Efficient Adsorption of Dyes Using Polyethyleneimine-Modified NH2-MIL-101 (Al) and its Sustainable Application as a Flame Retardant for an Epoxy Resin. ACS Omega 2020;5(50):32286–94.

[76] Jae J, Tompsett GA, Foster AJ, Hammond KD, Auerbach SM, Lobo RF, et al. Investigation into the shape selectivity of zeolite catalysts for biomass conversion. J Catal 2011;279(2):257–68.

[77] Lin Z-J, Zheng H-Q, Chen J, Zhuang W-E, Lin Y-X, Su J-W, et al. Encapsulation of phosphotungstic acid into metal–organic frameworks with tunable window sizes: Screening of PTA@MOF catalysts for efficient oxidative desulfurization. Inorg Chem 2018;57(20):13009–19.

[78] Bromberg L, Diao Y, Wu H, Speakman SA, Hatton TA. Chromium(III) Terephthalate Metal Organic Framework (MIL-101): HF-Free Synthesis, Structure, Polyoxometalate Composites, and Catalytic Properties. Chem Mater 2012;24(9):1664–75.

[79] Navarro-Sánchez J, Almora-Barrios N, Lerma-Berlanga B, Ruiz-Pernía JJ, Lorenz-Fonfria VA, Tuñón I, et al. Translocation of enzymes into a mesoporous MOF for enhanced catalytic activity under extreme conditions. Chem Sci 2019;10(14):4082–8.

[80] Maksimchuk NV, Timofeeva MN, Melgunov MS, Shmakov AN, Chesalov YA, Dybtsev DN, et al. Heterogeneous selective oxidation catalysts based on coordination polymer MIL-101 and transition metal-substituted polyoxometalates. J Catal 2008;257(2):315–23.

[81] Sun C-Y, Liu S-X, Liang D-D, Shao K-Z, Ren Y-H, Su Z-M. Highly stable crystalline catalysts based on a microporous metal− organic framework and polyoxometalates. J Am Chem Soc 2009;131(5):1883–8.

[82] Li X, Guo W, Gao X, Yue X. Phosphotungstic acid encapsulated in MIL-53(Fe) as efficient visible-light photocatalyst for rhodamine B degradation. Environ Prog Sustainable Energy 2017;36(5):1342–50.

[83] Hall JN, Bollini P. Metal–organic framework MIL-100 catalyzed acetalization of benzaldehyde with methanol: Lewis or Brønsted acid catalysis? ACS Catal 2020;10(6):3750–63.

[84] Zheng X-X, Fang Z-P, Dai Z-J, Cai J-M, Shen L-J, Zhang Y-F, et al. Iron-based metal–organic frameworks as platform for H_2S selective conversion: Structure-dependent desulfurization activity. Inorg Chem 2020;59(7):4483–92.

[85] Volkringer C, Leclerc H, Lavalley J-C, Loiseau T, Férey Gérard, Daturi M, et al. Infrared spectroscopy investigation of the acid sites in the metal–organic framework aluminum trimesate MIL-100 (Al). J Phys Chem C 2012;116(9):5710–9.

[86] Leclerc H, Vimont A, Lavalley J-C, Daturi M, Wiersum AD, Llwellyn PL, et al. Infrared study of the influence of reducible iron (III) metal sites on the adsorption of CO, CO_2, propane, propene and propyne in the mesoporous metal–organic framework MIL-100. Phys Chem Chem Phys 2011;13(24):11748. https://doi.org/10.1039/c1cp20502a.

[87] Herbst A, Khutia A, Janiak C. Brønsted instead of Lewis acidity in functionalized MIL-101Cr MOFs for efficient heterogeneous (nano-MOF) catalysis in the condensation reaction of aldehydes with alcohols. Inorg Chem 2014;53(14):7319–33.

[88] Hall JN, Bollini P. Metal-Organic Framework MIL-100 Catalyzed Acetalization of Benzaldehyde with Methanol: Lewis or Brønsted Acid Catalysis? ACS Catal 2020;10(6):3750–63.

[89] Vimont A, Goupil J-M, Lavalley J-C, Daturi M, Surblé S, Serre C, et al. Investigation of acid sites in a zeotypic giant pores chromium (III) carboxylate. J Am Chem Soc 2006;128(10):3218–27.

[90] Juan-Alcañiz J, Goesten M, Ramos-Fernandez E, Gascon J, Kapteijn F. Towards efficient polyoxometalate encapsulation in MIL-100 (Cr): Influence of synthesis conditions. New J Chem 2012;36(4):977–87.

[91] Patil SKR, Lund CRF. Formation and growth of humins via aldol addition and condensation during acid-catalyzed conversion of 5-hydroxymethylfurfural. Energy Fuels 2011;25(10):4745–55.

[92] Maksimchuk NV, Kholdeeva OA, Kovalenko KA, Fedin VP. MIL-101 Supported Polyoxometalates: Synthesis, Characterization, and Catalytic Applications in Selective Liquid-Phase Oxidation. Isr J Chem 2011;51(2):281–9.

[93] Song J, Luo Z, Britt DK, Furukawa H, Yaghi OM, Hardcastle KI, et al. A multiunit catalyst with synergistic stability and reactivity: a polyoxometalate–metal organic framework for aerobic decontamination. J Am Chem Soc 2011;133(42):16839–46.

[94] Hou Q, Li W, Zhen M, Liu L, Chen Y, Yang Q, et al. An ionic liquid–organic solvent biphasic system for efficient production of 5-hydroxymethylfurfural from carbohydrates at high concentrations. RSC Adv 2017;7(75):47288–96.

[95] Zhao P, Cui H, Zhang Y, Zhang Y, Wang Y, Zhang Y, et al. Synergetic Effect of Brønsted/Lewis Acid Sites and Water on the Catalytic Dehydration of Glucose to 5-Hydroxymethylfurfural by Heteropolyacid-Based Ionic Hybrids. ChemistryOpen 2018;7(10):824–32.

[96] Li H, Yang S. Catalytic Transformation of Fructose and Sucrose to HMF with Proline-Derived Ionic Liquids under Mild Conditions. Int J Chem Eng 2014;2014:1–7.

[97] Kumar K, Dahiya A, Patra T, Upadhyayula S. Upgrading of HMF and Biomass-Derived Acids into HMF Esters Using Bifunctional Ionic Liquid Catalysts under Solvent Free Conditions. ChemistrySelect 2018;3(22):6242–8.

[98] Xu Z, Yang Y, Yan P, Xia Z, Liu X, Zhang ZC. Mechanistic understanding of humin formation in the conversion of glucose and fructose to 5-hydroxymethylfurfural in [BMIM]Cl ionic liquid. RSC Adv 2020;10(57):34732–7.

[99] Tsilomelekis G, Orella MJ, Lin Z, Cheng Z, Zheng W, Nikolakis V, et al. Molecular structure, morphology and growth mechanisms and rates of 5-hydroxymethyl furfural (HMF) derived humins. Green Chem 2016;18(7):1983–93.

[100] Hou Q, Qi X, Zhen M, Qian H, Nie Y, Bai C, et al. Biorefinery roadmap based on catalytic production and upgrading 5-hydroxymethylfurfural. Green Chem 2021;23(1):119–231.

[101] Pidko E, Degirmenci V, vanSanten R, Hensen EM. Glucose activation by transient Cr2+ dimers. Angew Chem Int Ed 2010;122(14):2584–8.

[102] Pidko EA, Degirmenci V, Hensen EJM. On the mechanism of Lewis acid catalyzed glucose transformations in ionic liquids. ChemCatChem 2012;4(9):1263–71.

[103] Yang G, Pidko EA, Hensen EJM. The mechanism of glucose isomerization to fructose over Sn-BEA zeolite: a periodic density functional theory study. ChemSusChem 2013;6(9):1688–96.

[104] Tangsermvit V, Pila T, Boekfa B, Somjit V, Klysubun W, Limtrakul J, et al. Incorporation of Al3+ Sites on Brønsted Acid Metal-Organic Frameworks for Glucose-to-Hydroxylmethylfurfural Transformation. Small 2021;17(22):2006541.

[105] Newth F. The formation of furan compounds from hexoses. Adv Carbohyr Chem 1951;6:83–106.

[106] Antal MJ, Mok WSL, Richards GN. Mechanism of formation of 5-(hydroxymethyl)-2-furaldehyde from D-fructose and sucrose. Carbohyd Res 1990;199(1):91–109.

[107] Teong SP, Yi G, Zhang Y. Hydroxymethylfurfural production from bioresources: past, present and future. Green Chem 2014;16(4):2015–26.

[108] Li X, Peng K, Liu X, Xia Q, Wang Y. Comprehensive Understanding of the Role of Brønsted and Lewis Acid Sites in Glucose Conversion into 5-Hydromethylfurfural. ChemCatChem 2017;9(14):2739–46.

[109] Tangsermvit V, Pila T, Boekfa B, Somjit V, Klysubun W, Limtrakul J, et al. Incorporation of Al^{3+} sites on Brønsted acid metal–organic frameworks for glucose-to-hydroxylmethylfurfural transformation. Small 2021;17(22):2006541. https://doi.org/10.1002/smll.v17.2210.1002/smll.202006541.

[110] Choudhary V, Mushrif SH, Ho C, Anderko A, Nikolakis V, Marinkovic NS, et al. Insights into the interplay of Lewis and Brønsted acid catalysts in glucose and fructose conversion to 5-(hydroxymethyl) furfural and levulinic acid in aqueous media. JACS 2013;135(10):3997–4006.

[111] Férey G, Mellot-Draznieks C, Serre C, Millange F, Dutour J, Surblé S, et al. A chromium terephthalate-based solid with unusually large pore volumes and surface area. Science 2005;309(5743):2040–2.

[112] Luo Q-xing, Song X-dan, Ji M, Park S-E, Hao C, Li Y-qin. Molecular size-and shape-selective Knoevenagel condensation over microporous $Cu_3(BTC)_2$ immobilized amino-functionalized basic ionic liquid catalyst. Appl Catal, A 2014;478:81–90.

[113] Hwang Y, Hong D-Y, Chang J-S, Jhung S, Seo Y-K, Kim J, et al. Amine grafting on coordinatively unsaturated metal centers of MOFs: consequences for catalysis and metal encapsulation. Angew Chem Int Ed 2008;47(22):4144–8.

[114] Qu Y, Zhao Y, Xiong S, Wang C, Wang S, Zhu L, et al. Conversion of Glucose into 5-Hydroxymethylfurfural and Levulinic Acid Catalyzed by SO42−/ZrO2 in a Biphasic Solvent System. Energy Fuels 2020;34(9):11041–9.

[115] Dijkmans J, Gabriëls D, Dusselier M, de Clippel F, Vanelderen P, Houthoofd K, et al. Productive sugar isomerization with highly active Sn in dealuminated β zeolites. Green Chem 2013;15(10):2777. https://doi.org/10.1039/c3gc41239c.

[116] Tao M, Xue L, Sun Z, Wang S, Wang X, Shi J. Tailoring the synergistic Bronsted-Lewis acidic effects in heteropolyacid catalysts: Applied in esterification and transesterification reactions. Sci Rep 2015;5(1):13764.
[117] Liu N, Pu X, Wang X, Shi L. Study of alkylation on a Lewis and Brønsted acid hybrid catalyst and its industrial test. J Ind Eng Chem 2014;20(5):2848–57.
[118] Li B, Leng K, Zhang Y, Dynes JJ, Wang J, Hu Y, et al. Metal–organic framework based upon the synergy of a Brønsted acid framework and Lewis acid centers as a highly efficient heterogeneous catalyst for fixed-bed reactions. J Am Chem Soc 2015;137(12):4243–8.